Accepted Manuscript

On the thermal stability of the nanostructured tungsten coatings

N. Gordillo, C. Gómez de Castro, E. Tejado, J.Y. Pastor, G. Balabanian, M. Panizo-Laiz, R. Gonzalez-Arrabal, J.M. Perlado, J. del Rio

PII: S0257-8972(17)30684-9
DOI: doi: 10.1016/j.surfcoat.2017.06.070
Reference: SCT 22481

To appear in: *Surface & Coatings Technology*

Received date: 3 March 2017
Revised date: 25 June 2017
Accepted date: 26 June 2017

Please cite this article as: N. Gordillo, C. Gómez de Castro, E. Tejado, J.Y. Pastor, G. Balabanian, M. Panizo-Laiz, R. Gonzalez-Arrabal, J.M. Perlado, J. del Rio , On the thermal stability of the nanostructured tungsten coatings, *Surface & Coatings Technology* (2017), doi: 10.1016/j.surfcoat.2017.06.070

This is a PDF file of an unedited manuscript that has been accepted for publication. As a service to our customers we are providing this early version of the manuscript. The manuscript will undergo copyediting, typesetting, and review of the resulting proof before it is published in its final form. Please note that during the production process errors may be discovered which could affect the content, and all legal disclaimers that apply to the journal pertain.

ACCEPTED MANUSCRIPT

On the thermal stability of the nanostructured tungsten coatings

N. Gordillo[1,*], C. Gómez de Castro[2], E. Tejado[3], J.Y. Pastor[3], G. Balabanian[1,4], M. Panizo-Laiz[1], R. Gonzalez-Arrabal[1], J. M. Perlado[1] and J. del Rio[5]

[1]*Instituto de Fusión Nuclear, ETSI de Industriales, Universidad Politécnica de Madrid, C/ José Gutiérrez Abascal, 2, E-28006 Madrid, Spain.*

[2]*Departamento de Ciencia de Materiales e Ingeniería Metalúrgica, Facultad de CC. Químicas, Universidad Complutense de Madrid, Ciudad Universitaria s/n, E-28040 Madrid, Spain.*

[3]*Departmento de Ciencia de los Materiales-CIME , ETSI de Caminos, Canales y Puertos, Universidad Politécnica de Madrid, C/ Profesor Aranguren 3,E- 28040, Madrid, Spain*

[4]*Carl Zeiss Microscopy GmbH, Carl-Zeiss-Straße 22, 73446 Oberkochen, Germany.*

[5]*Departamento de Física de Materiales, Facultad de CC. Físicas, Universidad Complutense de Madrid, Ciudad Universitaria s/n, E-28040 Madrid, Spain.*

ACCEPTED MANUSCRIPT

[*] Current address: Departamento de Física Aplicada, Universidad Autónoma de Madrid, E-28049 Madrid Spain

ACCEPTED MANUSCRIPT

Abstract

Tungsten is a candidate to be used as plasma facing materials in future fusion nuclear reactors. There, the material has to withstand large radiation fluxes and thermal loads. Nowadays, nanostructured tungsten (NW) seems to exhibit a better radiation-resistance than the coarse grained. However, the thermal stability of NW is still an open question. On these bases, the thermal stability of NW coatings is studied in the temperature range from 1000 to 1473 K. For this purpose, Samples were isothermally annealed in vacuum at temperatures from 298 to 1473 K. The morphological and microstructural properties of the samples were characterized by atomic force microscopy (AFM), scanning electron microscopy (SEM) and X-Ray diffraction (XRD), respectively. For T<1000 K nanostructured are preserved and only a small reduction in the internal stress of the films is observed. For T> 100 K, nanostructures start to grow in a bimodal fashion with activation energy of 0.259 eV, reaching a submicron-sized threshold at T ≈ 1473 K.

Keynotes: thermal stability, thermo-diffraction, nanostructured tungsten, HiPIMS

ACCEPTED MANUSCRIPT

ACCEPTED MANUSCRIPT

1. Introduction:

Nanostructured materials (NMs), which are made of many interfaces forming a system with a large density of grain boundaries (GBs), offer a potential alternative to the microcrystalline counterpart. They are increasingly being used, in particular in the field of nuclear fusion energy, due to their larger radiation resistance and advantageous physical and mechanical properties [1–7]. Additionally, the inherently small size of NMs, makes them exceptional in other applications such as charge transport [8] or corrosion resistance coatings [9].

In future fusion devices, tungsten (W) is the material proposed as plasma facing material (PFM) due to its excellent properties: high melting point, good thermal conductivity, low thermal expansion, high strength at high temperatures and high sputtering threshold energy [10–13]. However, there are still some requirements that need to be satisfied such as to improve the radiation-resistant of the material and/or its mechanical properties. On these bases, nanostructured materials could be an option to improve performance. i.e. previous works suggest that mechanical response of W could be further improved when it is doped with nanoparticles or nanocomposites like K, Y_2O_3 or Re [3,4,14,15]. Other studies suggest that nanostructured tungsten (NW) exhibit a larger radiation-resistance than coarse-grained tungsten since grain boundaries contribute to (i) annihilation of Frenkel-pairs (self-healing behaviour), and (ii) pinning centres for light species [16–22]. These two facts may delay the appearance of blistering and exfoliation effects to larger radiation fluencies. Nevertheless, beyond the improvements that NMs offer in many applications, they are naturally unstable. This means that under certain circumstance, irradiation or temperature, can activate grain growth, follow-on a partial or total annihilation of nanostructure and loss of the

ACCEPTED MANUSCRIPT

associated properties [23]. According to literature, the base temperature as estimated by finite element methods at the PFM surface of the European designed of a nuclear fusion reactor can reach up to 900 K [24]. Therefore, the study of the thermal stability of NW is a key point, since at this temperature grain growth should be excluded for a proper performance of the reactor.

In this work we study the thermal stability of nanostructured tungsten (NW) coatings in the temperature range from 298 to 1473 K, determining the activation energy of the nanograins to start growing.

2. Experimental procedure:

Nanostructured tungsten (NW) coatings with a thickness of 5 μm were deposited on commercial tungsten polished substrates with a thickness of 3 mm and on a Si (100) single side polished for easy further cross-sectional characterization.

Prior to deposition, the W substrates were mechanically polished by using napless synthetic cloth. For the first rough polishing step, a 0.5 μm colloidal alumina was used. The second polishing was done with a 0.03 μm colloidal alumina. Then, all substrates underwent cleaning processes, which consist of the following steps: (i) washing the substrate with ultra-pure water soap solution, (ii) bathing in acetone during five minutes, (iii) immersion in an isopropanol ultrasound bath, and (iv) drying by blowing with nitrogen gas. Moreover, once introduce into the vacuum chamber all the substrates were etched during 30 min in an Ar atmosphere by biasing them using a DC-pulsed voltage of 600V at a frequency of 150 KHz. The Ar pressure was 6.5×10^{-3} mbar.

ACCEPTED MANUSCRIPT

The deposition setup consists of a high vacuum chamber (main chamber) with a base pressure in the 10^{-8} mbar range. Before the deposition of the samples, the W cathode was cleaned by argon plasma etching during five minutes in order to avoid contamination by the possible target oxidation.

NW coatings were deposited by combining two growth methods: i) High Power Impulse Magnetron Sputtering (HiPIMS) and ii) Direct Current Magnetron Sputtering (DCMS). We have used two methods (HiPIMS and DCMS) in order to improve the adhesion of the coating on the substrate. HiPIMS is used with two purposes: i) surface pretreatment and ii) deposition of a compliant layer of few hundreds of nanometres. According to the literature [25,26], HiPiMS is well suited for a surface pretreatment aimed to remove the natural oxide layer that exists on most materials. The compliant layer favours the stability of the coating when you want deposit few microns in thickness. NW Coatings were deposited at room temperature from a pure W commercial target (99.95 %) placed in 2-inch diameter magnetron designed and manufactured by Nano4Energy SLNE [27] in the presence of a high purity Ar atmosphere (99.9999 %).

It is worthwhile to mention that all the samples studied were simultaneously deposited. Firstly, a complitan layer with a thickness of few hundreds of nanometers is deposited by HiPIMS during 10 min. HiPIMS deposition took place in DC-pulsed configuration in a pure argon atmosphere at a pressure of 9.5×10^{-3} mbar. The pulse width was 100 µs, the frequency 150 kHz, the peak voltage 450V, and the plasma current 16 A. Then, the system was immediately set to a DCMS mode for 120 minutes. In this mode, the plasma current and the voltage were 0.19A and 250V, respectively and the Ar gas pressure was 8×10^{-3} mbar. The cathode-sample distance was kept constant at 8 cm. More information

ACCEPTED MANUSCRIPT

about the deposition setup and the optimisation of tungsten nanostructured coatings can be found in reference [28].

The microstructure of the samples was characterised by X-ray diffraction (XRD) measurements. The diffractometer used was the multi-purpose PANalytical X'Pert PRO MPD with a $Cu_{K\alpha}$ (λ=0.15405 nm) radiation source provided with an oven Anton Paar HTK1200. In order to study the influence of the annealing treatment on the nanostructures, the diffractograms were measured at different temperatures from room temperature (RT, 298 K) up to 1473 K. The heating rate was 288 K/min. Before each measurement, we waited for 10 minutes until the temperature reach a stable value. The measurements time for each diffractogram was about 32 minutes. All the diffractograms were acquired under high vacuum conditions at a pressure lower than 10^{-6} mbar. Once the last measured was captured, the sample was cooled down in vacuum up to reaching RT. Rietveld structural refinements of the XRD spectra were performed by the TOPAS (TransistOr Parameter Scalable model) software developed by IMST GmbH [29]. In order to study the morphology evolution with temperature, we heat the two samples following the same thermal treatment as the one described for the diffractometer at two intermediate temperatures, 873 and 1173 K. Therefore, we have at least four samples at different temperatures (RT, 837, 1173 and 1473 K) in order to study the thermal stability of the nanostructured.

The morphology of the film surface and the grain size were imaged by means of atomic force (AFM) and scanning electron (SEM) microscopes. The AFM was operated in the dynamic mode. A Si tip of 20 nm diameter and 60–70 kHz, special for this operation mode was employed. Topography data and root mean square (RMS) roughness were analysed by the free software WsxM, from Nanotec Electronics S.L [30]. The SEM

ACCEPTED MANUSCRIPT

images were obtained with a ZEISS AURIGA microscope (Carl Zeiss, Oberkochen, Germany).

3. Results and discussions

The sample codes, the total time up to reach a given temperature, the average grain sizes and the RMS roughness of each studied sample are summarised in TableI. The NW_AD is the as deposited sample and the NW_873, NW_1173 and NW_1473 are the samples annealed at 873, 1173 and 1473 K, respectively. The values of average grain sizes and the RMS are from the results shown in *section 3.3*.

In general, we consider two values for the grain size: i) the average value which is the arithmetic mean of the values obtained over 60 grains and ii) the maximum grain size which is the maximum size observed in the analysed images.

Table 1: Brief overview of the of the temperature and time used for the annealing treatments, average grain sizes and RMS of the samples studied in this work:

Sample code	NW_AD	NW_873	NW_1173	NW_1473
Temperature (K)	298	873	1173	1473
t (time treatment)	0	3h 48min	5h 42 min	7h 36 min
Average grain size (nm)	211	234	261	295
Maximum grain size (nm)	329	346	572	735
rms (nm)	12	12	16	30

3.1 Structural characterization

The microstructure of the samples was characterized prior to and after annealing by XRD from the θ –2θ scans. Results are shown in Figure 1. As-deposited coatings

ACCEPTED MANUSCRIPT

exhibit four Bragg peaks corresponding to the α-{110}, α-{200}, α-{211} and α-{220} reflections of the thermodynamically stable body-centred cubic (bcc) α–W phase [28]. No β–W phase signed is detected in our experiment. These results agree quite well with those previously reported in literature which show that thick samples deposited at room temperature exhibit only the α–W phase [5,28,31,32] whereas the metastable β–W phase is normally seen for thin films (< 50 nm). For annealed samples, some four peaks are observed, independently of annealing temperature, which indicates that the thermal treatments do not promote the formation of new phases in the studied temperature range.

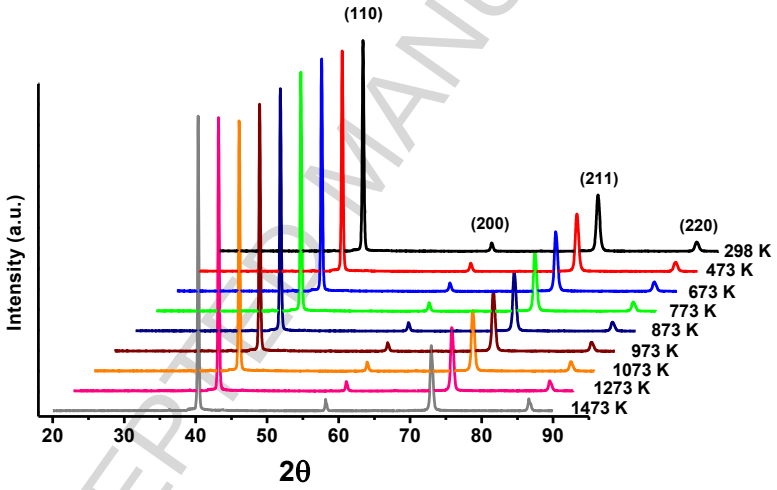

Figure 1: θ-2θ diffractograms from 298 K to 1473 K. The reflection axes corresponding to the α-W phase are indicated in the figure.

Rietveld refinement diffractograms were performed by means of TOPAS software. For Rietveld the annealing temperature, deformation, height, sample position and texture effects were considered. Figure 2a shows the calculated relative increase in the lattice parameters by taking the as-deposited sample as reference. As it can be seen, experimental data are linearly well fitted. The fit slope corresponds to the linear expansion coefficient. The calculated value for this

ACCEPTED MANUSCRIPT

slope is 5.0×10^{-6} K^{-1}, which is very close to the linear expansion coefficient reported for tungsten (4.5×10^{-6} K^{-1}) [33].

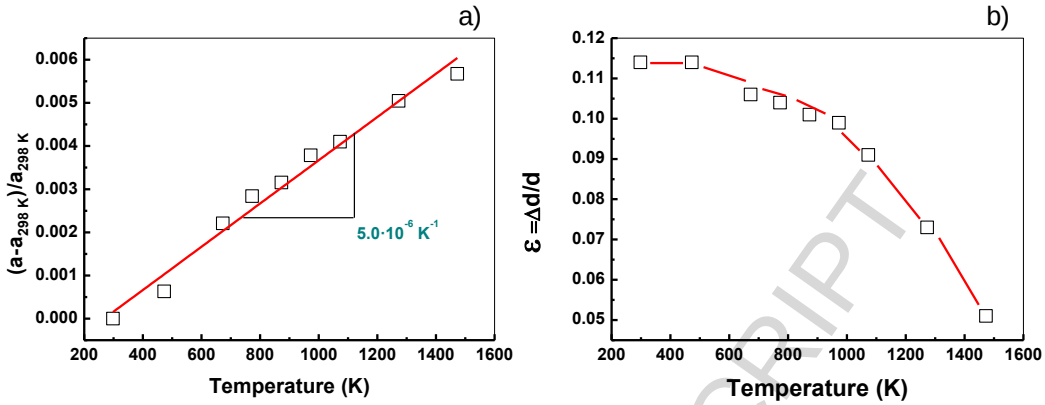

Figure 2:a) The relative lattice parameter as a function of temperature. b)The deformation parameter (ε) calculated from the Rietveld analysis as a function of temperature.

The micro-deformation parameter (ε) resulting from the X-Ray diffractograms refinement shows that the stress present in the as-deposited sample was relaxed by a factor of ~2 by the annealing treatment. Two different regimes can be observed in the evolution of ε with temperature. From RT until 1000 K, the deformation parameter softly decreases, which indicates a gradual relaxation in the residual stress of the NW coating. For temperatures higher than1000 K, the residual stress drastically decreases when increasing temperature, and ε is reduced in more than 55% with respect to the initial value. This result suggests that the residual stress present in the layer has been almost removed by the thermal treatment. These results agree with that previously reported in literature in which it is shown that the last tungsten recovery stage takes place in the temperature range from 1173 K to 1673 K and it is associated with the crystallisation processes [34]. Thus, this is an indication that a recrystallization would be produced in the NW layer between 1000 K and 1473 K, which may account for the

ACCEPTED MANUSCRIPT

observed decreases of the residual stresses. This hypothesis is further supported by the enhancement of the mean grain size observed by SEM (see section 3.3).

3.2 Texture analysis

Rietveld analyses of diffractograms reveal that the sample is highly textured with the (111) planes parallel to the growth direction of the layer. The texture degree parameter introduced by Rietveld refinement remains almost constant over the entire temperature interval, which points out that layer texture, was not affected by the annealing. A detailed texture analysis of both, the as-deposited and annealed at 1473 K samples confirm this result. As it is seen in Figure 3a, the pole figure for the (222) reflection shows that for the as-deposited sample, grains are growing along the <111> direction. The asymmetry observed in this figure may indicate that the growing direction of grains is tilted about 10 degrees from the perpendicular to the sample surface and spatially distributed in a fan of around 50 degrees in aperture. From the pole figures for the sample annealed at 1473 K (Figure 3b) we conclude that texture is not changed by the annealing, as the Rietveld analysis shows. It is also important to stand out that the pole figures from the (222) before and after annealing reflection are very similar which points out that the columnar shape is preserved during the thermal treatment. Only some differences can be observed between pole figures in the as-deposited and annealed samples in the (110), (211) and (321) reflection, which are due to the recrystallization of the samples.

ACCEPTED MANUSCRIPT

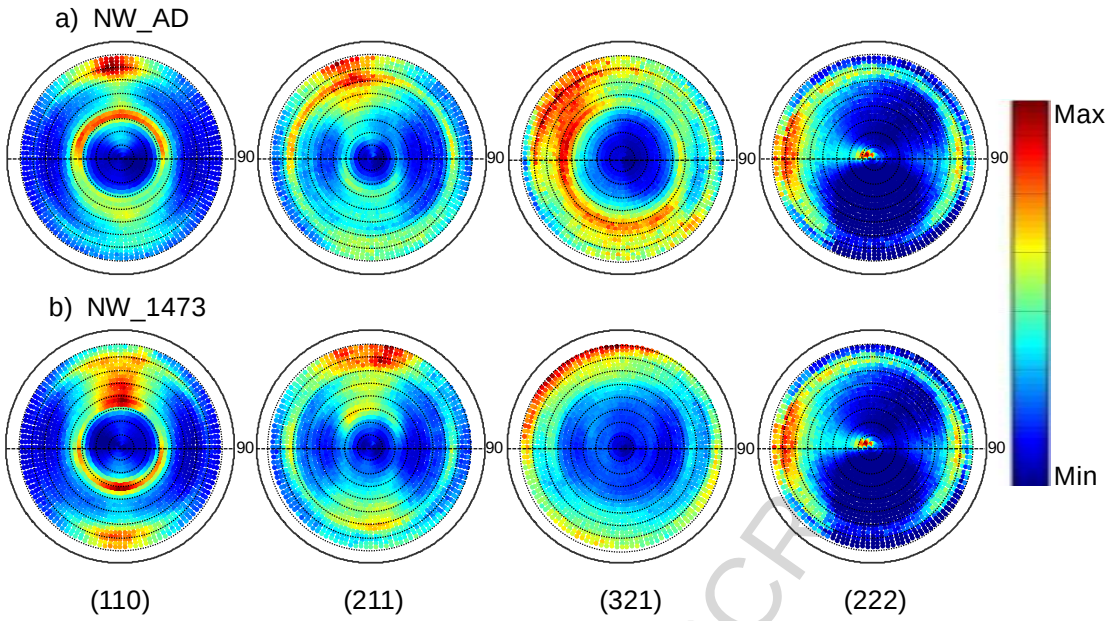

Figure 3: Pole figures from the (110), (211), (321) and (222) reflections for a) the NW_AD and b) NW_1473 samples.

3.3 Characterization of the grain growth and grain stability

Prior to any thermal treatment, the surface morphology and thickness of the coating were evaluated from top-view and cross-section SEM images respectively. In order to do that, the NW deposited on (100) Si was used since it does not need any preparation requirements for the cross-section image acquisition. Figure 4a and b show that the samples have a smooth surface and are made of nanostructures with a columnar shape that grow perpendicular to the substrate. The column diameter is about 200 nm and the thickness of the coating is about 5 µm, being in agreement with our previous results [28].

ACCEPTED MANUSCRIPT

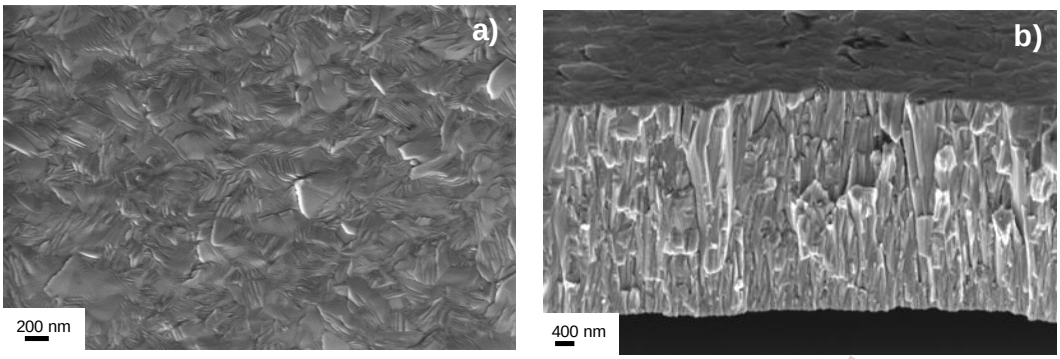

Figure 4:a) top-view and b) cross-sectional SEM images of the as-deposited NW coatings sputtered on (100) Si.

In order to evaluate if the thermal treatment has induced any mechanism to favour the grain growth, the surface topography and morphology were evaluated from the images acquired by means of AFM and SEM. Figure 5 shows the surface topography characterised by AFM for the as-deposited and annealed layers. Changes in the grains are visible in the topography images. The as-deposited sample (NW_AD) exhibits grains with a size of about 200 nm in diameter and which in turn are formed by folds of few nm. Then, as soon as the annealing temperature is increased, a considerable enlargement of some grains can be observed. One grain may grow into another whilst being consumed from the other side to become a bigger grain. The grain growth has been observed previously in the case of nanostructured tungsten prepared by powder metallurgy [35]. Butler *et al.* indicates that the thermal stability changes significantly based on milling conditions. They observe a gradual increase in grain size throughout the temperatures range from 1073 to 1673 K, while a reduced in the grain growth from 1273 to 1473 K depending on sintering process. They attribute this result to the Zener pinning from the dispersoid phase, which caused a reduction in the grain boundary mobility.

ACCEPTED MANUSCRIPT

By comparing the root mean square (RMS) roughness of the as-deposited (Figure 5a) to that of the annealed samples (Figure 5b-d) one observes that it rises when increasing temperature being 12 and 30 nm for the as-deposited and annealed at 1473K layer, which is compatible with the previously described recrystallization of the sample.

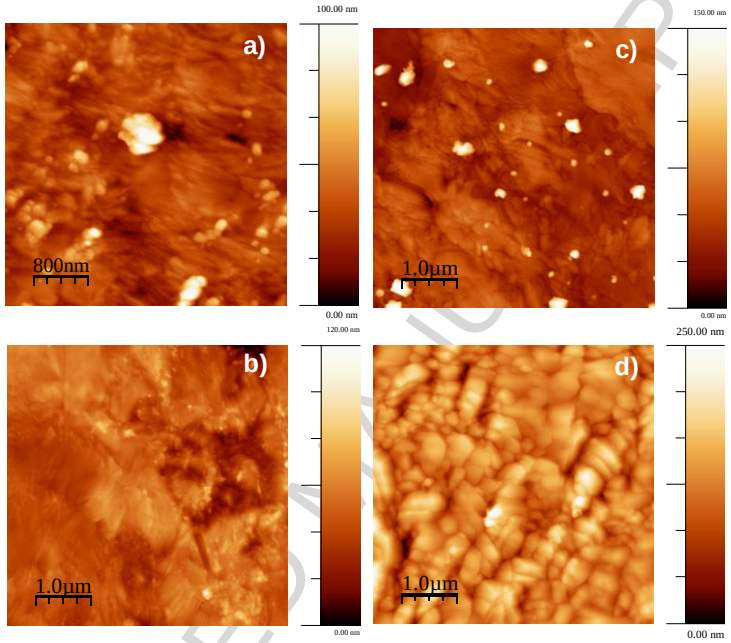

Figure 5: AFM images showing the surface topography and morphology of the NW coatings a) as-deposited, rms =12 nm and annealed b) at 873K, rms = 12 nm, c) at 1173 K, rms = 16 nm and d) at 1473 K, rms = 30 nm.

Figure 6 shows SEM images illustrating the morphological surface evolution from RT up to 1473 K. The top-view images are represented together with the histograms evaluated from each picture, which indicates the grain size distribution for every annealed layer. As in the AFM images, a clear change in the grain shape and size is seen. The histograms indicate that on average, grains are nearly stable at annealing temperatures lower than 1173 K, starting to grow at higher temperatures up to reaching

ACCEPTED MANUSCRIPT

a size of 800 nm for the sample annealed at 1473 K. However, only a small fraction of the grains has grown (less than 10%), while the size of many of them still remain being 200-300 nm. Eventually, these large grains impinge on no-growth grains, which may then start growing. In this process, called "discontinuous process" [36], a few grains in the microstructure grow and consume the matrix of smaller grains developing into a bimodal grain size distribution.

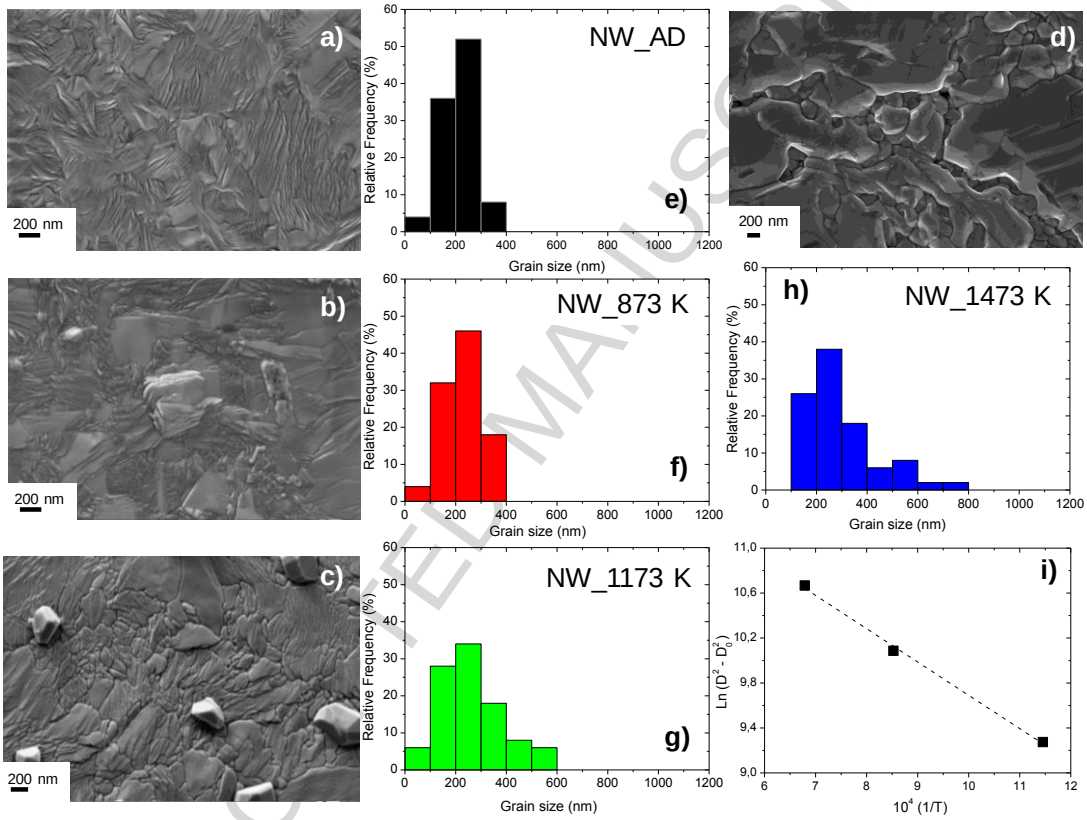

Figure 6:(a-d) Top-view SEM images and (e-f) histograms representing the grain size distribution on the sample surface for NW coatings: a,e) as-deposited, b,f) annealed at 873 K, c,g) annealed at 1173 K and d,h) annealed at 1473 K. i) Arrhenius plotting of the temperature dependence of the grain growth, from equation 1.

ACCEPTED MANUSCRIPT

The grain growth dependency on temperature and time induced by isothermal treatment can be studied by applying the classical approach for the kinetics of normal grain growth [37], described by equation (1):

$$D^2 - D_0^2 = K_0 e^{\left(-\frac{Q}{k_B T}\right)} t \quad (1)$$

where D_0 is the average grain size of the as-deposited sample, i.e. the initial size, D is the average grain size at time t, Q is the activation enthalpy for grain growth, T the temperature, k_B the Boltzmann constant and K_0 a rate constant. By fitting the experimental data represented in Figure 6 i) to Eq. (1), we obtain the activation enthalpy Q from the slope of the curve and the rate constant K_0 from the intersection with the Y-axis. The analysis results in a Q = 25±1 *kJ/mol* (0.259±0.01 *eV*) and K_0 = 11 nm^2/s.

In general, the grain growth occurs due to the movement of grain boundaries, where the boundary movement can be discontinuous, and change the direction of the motion unexpectedly. This activation enthalpy is related to the activation energy for boundary mobility which theoretically should be near to the self-diffusion energy although frequently that is not the case [36,38,39]. For example, for pure coarse-grained tungsten, the activation enthalpy for self-diffusion is within the range of 586-628 *kJ/mol* for single crystal, and 502-586 *kJ/mol* for polycrystalline tungsten [33], whereas the activation enthalpy for grain growth for a polycrystalline tungsten is 210.7±13.2 *kJ/mol* [36]. In the case of the nanocrystalline tungsten, the activation energy shows a strong correlation to the grain size. It has been reported to change from 400 to 900 *kJ/mol* for powder samples with a grain size of 135 and 650 nm, repectively [35]. Butler *et al.* [43] report a similar correlation. They observed that the activation energy for nanostructured tungsten prepared by powder metallurgy varies from 400 – 1000 *kJ/mol* for sample with

ACCEPTED MANUSCRIPT

a grain size of 150 and 550 nm. Other authors found lower activation energy (183±6 *kJ/mol*) for the sub-micron grained structure of tungsten doped with Y_2O_3[3]. However, Y_2O_3 addition in coarse-grained tungsten inhibits the growth, for which the activation energy increases up to 240±11 *kJ/mol*. In other systems like nanocrystalline Fe prepared by pulsed electron deposition, the activation energy is also low (98 *kJ/mol*) [40]. In fact, Natter *et al.* observe two regimes: i) high temperature regime, where Q = 173 *kJ/mol* and ii) low temperature regime, where Q = 98 *kJ/mol*. In the regime i), the Q value is in agreement with the activation energy of the grain-boundary self-diffusion coefficient of polycrystalline Fe, *Q* = 174.5 *kJ/mol* therefore, the system is out of the nanocrystalline size regime, i.e. sub-μ-regime. The diffusivity and growth kinetics in this regime correspond to those of polycrystalline materials. In the regime ii) the low Q value corresponds to the nanocrystalline size regime. Therefore, the differences can be explained considering that there are many factors which influence grain growth: temperature, impurities, initial size, texture, etc [38,39,41]. Our values and those reported in literature suggest a correlation between the initial grain size and the activation energy thus, the smaller the grain size, the lower the activation energy. Therefore, the low *Q* value that we have obtained seems reasonable, since we are dealing with quite small grain sizes. This is an important parameter and should be considered in the manufacture of PFM or whatever application which involve the use of NW at high temperatures.

4. Conclusions

We study the thermal stability of nanostructured W. The thermo-diffraction analysis correlated with the increasing of the mean grain size observed by AFM and SEM reveals two behaviours in the microstructural stability:

ACCEPTED MANUSCRIPT

i) For temperatures lower than 1000 K the deformation parameter softly decreases when increasing temperature. No grain growth has been observed and stress present in the coatings is associated only with the fabrication method.

ii) For temperatures higher than 1000 K, the deformation parameter is reduced in more than 55% (1473 K) with respect to the initial value when the temperature increases indicating that the residual stress in the sample was almost removed. Grain growth is observed and the recrystallization develops into a bimodal grain distribution.

Finally, the activation energy for the grain growth of the nanostructures was calculated to be Q = 25±1 *kJ/mol* (0.259±0.01 *eV*) at temperatures around 1000 K, reaching a submicron-sized threshold at T ≤ 1473 K. These results indicate that the grain size of nanostructured W may be a point of concern if working as plasma facing material, since grain growth has been observed in a temperature range close to that for operation. Nevertheless, in order to have conclusive results, experiments about the thermal stability of W should be carried out under pulsed thermal loads with characteristics (pulse time and energy density) similar to those expected in nuclear fusion reactors. Such studies felt out of the scope of this paper.

ACCEPTED MANUSCRIPT

ACCEPTED MANUSCRIPT

Acknowledgments

Authors would like to thank the Centro de Apoyo a la Investigación (CAI) from the Excellence Moncloa-Campus placed at Madrid-Spain for the thermo-diffraction measurements and the AFM images. C.G.C, J.R and N.G gratefully acknowledges many fruitful discussions with Dr. Jose Antonio Jimenez from CENIM-CSIC about thermo-diffraction measurements and analysis. Research by NG is supported by MINECO (Spain) under project JdCI-2012-12652.This research was supported by Comunidad de Madrid (S2013/MIT-2862-MULTIMATCHALLENGE), Ministerio de Economía y Competitividad of Spain (MAT2015-70780-C4-4-P, ENE2015-70300-C3-3-R (Radiafus-4)).

ACCEPTED MANUSCRIPT

ACCEPTED MANUSCRIPT

Table caption:

Table I.- Brief overview of the of the temperature and time used for the annealing treatments, average grain sizes and RMS of the samples studied in this work:

Sample code	NW_AD	NW_873	NW_1173	NW_1473
Temperature (K)	298	873	1173	1473
t (time treatment)	0	3h 48min	5h 42 min	7h 36 min
Average grain size (nm)	211	234	261	295
Maximum grain size (nm)	329	346	572	735
rms (nm)	12	12	16	30

ACCEPTED MANUSCRIPT

ACCEPTED MANUSCRIPT

Figure captions:

Figure 1.-θ-2θ diffractograms from 298 K to 1473 K. The direction of the α-W diffracted peaks are indicated in the figure.

Figure 2.-a) The relative lattice parameter as a function of temperature. b) The deformation parameter (ε) as a function of temperature.

Figure 3.- Pole figures from the reflections (110), (211), (321) and (222) for a) the as-deposited and b) annealed at T = 1473 K samples.

Figure 4.-a) top-view and b) cross-section SEM images of the as-deposited NW coating.

Figure 5.- AFM images showing the surface topography and morphology of the NW coatings a) as-deposited, rms =12 nm and annealed b) at 873K, rms = 12 nm, c) at 1173 K, rms = 16 nm and d) at 1473 K, rms = 30 nm.

Figure 6.- (a-d) Top-view SEM images of NW coatings and (e-f) histograms representing the grain size distribution on the sample surface for: a, e) as-deposited, and annealed at b, f) 873 K, c, g) 1173 K and d, h) 1473 K samples. i) Arrhenius plotting of the temperature dependence of the grain growth, from equation 1.

ACCEPTED MANUSCRIPT

References:

[1] R.A. Andrievski, J. Mater. Sci. 49 (2014) 1449–1460.

[2] M. Zhang, B. Yang, J. Chu, T. Nieh, Scr. Mater. 54 (2006) 1227–1230.

[3] J. Martinez, B. Savoini, M.A. Monge, A. Muñoz, D.E.J. Armstrong, R. Pareja, Proc. 27th Symp. Fusion Technol. SOFT-27 Liège Belg. Sept. 24-28 2012 88 (2013) 2636–2640.

[4] T. Palacios, J. Reiser, J. Hoffmann, M. Rieth, A. Hoffmann, J.Y. Pastor, Int. J. Refract. Met. Hard Mater. 48 (2015) 145–149.

[5] V. Stelmakh, V. Rinnerbauer, J.D. Joannopoulos, M. Soljačić, I. Celanovic, J.J. Senkevich, C. Tucker, T. Ives, R. Shrader, J. Vac. Sci. Technol. Vac. Surf. Films 31 (2013) 061505.

[6] I.J. Beyerlein, A. Caro, M.J. Demkowicz, N.A. Mara, A. Misra, B.P. Uberuaga, Mater. Today 16 (2013) 443–449.

[7] W. Liu, Y. Ji, P. Tan, H. Zang, C. He, D. Yun, C. Zhang, Z. Yang, Materials 9 (2016) 105.

[8] H. Zheng, J.Z. Ou, M.S. Strano, R.B. Kaner, A. Mitchell, K. Kalantar-zadeh, Adv. Funct. Mater. 21 (2011) 2175–2196.

[9] J. Bhattarai, E. Akiyama, H. Habazaki, A. Kawashima, K. Asami, K. Hashimoto, Corros. Sci. 40 (1998) 757–779.

ACCEPTED MANUSCRIPT

[10] V. Barabash, G. Federici, R. Matera, A.R. Raffray, I.H. Teams, Phys. Scr. 1999 (1999) 74.

[11] M. Kaufmann, R. Neu, Fusion Eng. Des. 82 (2007) 521–527.

[12] R.E. Nygren, R. Raffray, D. Whyte, M.A. Urickson, M. Baldwin, L.L. Snead, J. Nucl. Mater. 417 (2011) 451–456.

[13] J. Alvarez, D. Garoz, R. Gonzalez-Arrabal, A. Rivera, M. Perlado, Nucl. Fusion 51 (2011) 053019.

[14] X. Tan, L. Luo, H. Chen, X. Zhu, X. Zan, G. Luo, J. Chen, P. Li, J. Cheng, D. Liu, Y. Wu, Sci. Rep. 5 (2015) 12755.

[15] D.E.J. Armstrong, X. Yi, E.A. Marquis, S.G. Roberts, J. Nucl. Mater. 432 (2013) 428–436.

[16] R. Gonzalez-Arrabal, M. Panizo-Laiz, N. Gordillo, E. Tejado, F. Munnik, A. Rivera, J.M. Perlado, J. Nucl. Mater. 453 (2014) 287–295.

[17] C.L. Guerrero, N. Gordillo, R. Iglesias, J.M. Perlado, C. Gonzalez, Model. Simul. Mater. Sci. Eng. 24 (2016) 045006.

[18] G. Valles, M. Panizo-Laiz, C. González, I. Martin-Bragado, R. González-Arrabal, N. Gordillo, R. Iglesias, C.L. Guerrero, J.M. Perlado, A. Rivera, Acta Mater. 122 (2017) 277–286.

[19] O. El-Atwani, J.A. Hinks, G. Greaves, S. Gonderman, T. Qiu, M. Efe, J.P. Allain, Sci. Rep. 4 (2014).

ACCEPTED MANUSCRIPT

[20] C. González, M. Panizo-Laiz, N. Gordillo, C.L. Guerrero, E. Tejado, F. Munnik, P. Piaggi, E. Bringa, R. Iglesias, J.M. Perlado, R. González-Arrabal, Nucl. Fusion 55 (2015) 113009.

[21] P.M. Piaggi, E.M. Bringa, R.C. Pasianot, N. Gordillo, M. Panizo-Laiz, J. del Río, C. Gómez de Castro, R. Gonzalez-Arrabal, J. Nucl. Mater. 458 (2015) 233–239.

[22] C. Guerrero, C. González, R. Iglesias, J.M. Perlado, R. González-Arrabal, J. Mater. Sci. 51 (2016) 1445–1455.

[23] D. Kaoumi, A.T. Motta, R.C. Birtcher, J. Appl. Phys. 104 (2008) 073525.

[24] D. Garoz, A.R. Páramo, A. Rivera, J.M. Perlado, R. González-Arrabal, Nucl. Fusion 56 (2016) 126014.

[25] M. Lattemann, A.P. Ehiasarian, J. Bohlmark, P.Å.O. Persson, U. Helmersson, Surf. Coat. Technol. 200 (2006) 6495–6499.

[26] A.P. Ehiasarian, J.G. Wen, I. Petrov, J. Appl. Phys. 101 (2007) 054301.

[27] Www.Nano4energy.Eu (n.d.).

[28] N. Gordillo, M. Panizo-Laiz, E. Tejado, I. Fernandez-Martinez, A. Rivera, J.Y. Pastor, C.G. de Castro, J. del Rio, J.M. Perlado, R. Gonzalez-Arrabal, Appl. Surf. Sci. 316 (2014) 1–8.

[29] TOPAS Software - Www.Topas.Imst.De, n.d.

ACCEPTED MANUSCRIPT

[30] I. Horcas, R. Fernández, J.M. Gómez-Rodríguez, J. Colchero, J. Gómez-Herrero, A.M. Baro, Rev. Sci. Instrum. 78 (2007).

[31] I.C. Noyan, T.M. Shaw, C.C. Goldsmith, J. Appl. Phys. 82 (1997) 4300–4302.

[32] S.M. Rossnagel, I.C. Noyan, J. C. Cabral, J. Vac. Sci. Technol. B Microelectron. Nanometer Struct. 20 (2002) 2047–2051.

[33] E. Lassner, W.-D. Schubert, Tungsten: Properties, Chemistry, Technology of the Elements, Alloys, and Chemical Compounds, Springer, United States of America, 1999.

[34] H. Schultz, Acta Metall. 12 (1964) 761–762.

[35] Brady Butler, Eric Klier, Micah Gallagher, Thermal Stability of Milled Nanocrystalline Tungsten Powders, Army Research Laboratory, Aberdeen Proving Ground, MD 21005, 2011.

[36] J. Almanstötter, M. Rühle, Int. J. Refract. Met. Hard Mater. 15 (1997) 295–300.

[37] H. Gleiter, Acta Mater. 48 (2000) 1–29.

[38] D. Raabe, Model. Simul. Mater. Sci. Eng. 15 (2007) 39.

[39] F.J. Humphreys, M. Hatherly, Recrystallization and Related Annealing Phenomena, 1st ed, Pergamon, Oxford, OX, UK ; Tarrytown, N.Y., U.S.A, 1995.

[40] H. Natter, M. Schmelzer, M.-S. Löffler, C.E. Krill, A. Fitch, R. Hempelmann, J. Phys. Chem. B 104 (2000) 2467–2476.

[41] H. Gleiter, Prog. Mater. Sci. 33 (1989) 223–315.

ACCEPTED MANUSCRIPT

Highlights:

- *In situ* thermodiffraction was used to study the stability of nanostructured tungsten.
- The diffractograms were measured from RT up to 1473 K.
- No grain growth is observed for temperatures lower than 1000 K.
- The recrystallization develops into a bimodal grain distribution for temperatures higher than 1000 K.

ACCEPTED MANUSCRIPT